

Quark flavor violation and axion-like particles from top-quark decays at the LHC

Kingman Cheung,^{a,b,c} Fei-Tung Chung,^{a,b} Giovanna Cottin,^{d,e} Zeren Simon Wang^{a,b}

^a*Department of Physics, National Tsing Hua University, Hsinchu 300, Taiwan*

^b*Center for Theory and Computation, National Tsing Hua University, Hsinchu 300, Taiwan*

^c*Division of Quantum Phases and Devices, School of Physics, Konkuk University, Seoul 143-701, Republic of Korea*

^d*Instituto de Física, Pontificia Universidad Católica de Chile, Avenida Vicuña Mackenna 4860, Santiago, Chile*

^e*Millennium Institute for Subatomic Physics at the High Energy Frontier (SAPHIR), Fernández Concha 700, Santiago, Chile*

E-mail: cheung@phys.nthu.edu.tw, feitung.chung@gapp.nthu.edu.tw,
gfcottin@uc.cl, wzs@mx.nthu.edu.tw

ABSTRACT: We study axion-like particles (ALPs) with quark-flavor-violating couplings at the LHC. Specifically, we focus on the theoretical scenario with ALP-top-up and ALP-top-charm interactions, in addition to the more common quark-flavor-diagonal couplings. The ALPs can thus originate from decays of top quarks which are pair produced in large numbers at the LHC, and then decay to jets. If these couplings to the quarks are tiny and the ALPs have $\mathcal{O}(10)$ GeV masses, they are long-lived, leading to signatures of displaced vertex plus multiple jets, which have the advantage of suppression of background events at the LHC. We recast a recent ATLAS search for the same signature and reinterpret the results in terms of bounds on the long-lived ALP in our theoretical scenario. We find that the LHC with the full Run 2 dataset can place stringent limits, while at the future high-luminosity LHC with 3 ab^{-1} integrated luminosity stronger sensitivities are expected.

Contents

1	Introduction	1
2	The ALP model with quark flavor violation	3
3	Experiment and simulation	5
3.1	The ATLAS DV+jets search	5
3.2	Simulation and computation	5
4	Numerical results	6
5	Summary and outlook	10
A	Recast of the DV+jets search	11

1 Introduction

In recent years, given the absence of any hints of heavy, promptly decaying, new fundamental particles since the observation of the Standard-Model (SM) Higgs boson at the LHC [1, 2], more attention has been given to non-traditional, possible forms of new physics (NP) beyond the Standard Model (BSM), such as light and feebly interacting particles [3, 4]. Such types of new particles are predicted widely in various NP models and are often long-lived, such that once produced they travel a macroscopic distance before decaying into either SM or other BSM particles. In general, if such long-lived particles (LLPs) (see Refs. [5–8] for recent reviews) are produced at the LHC, they can have escaped the past searches because these searches apply search strategies focusing on traditional signatures. Given this possible reason of having missed discovery of new physics at the LHC, novel search strategies have been proposed and applied. For instance, both ATLAS and CMS have published various types of LLP searches in recent years, targeting specific LLP collider signatures such as disappearing track [9, 10], displaced vertices and missing transverse momentum [11, 12], displaced vertex and a lepton [13], displaced leptons [14, 15], and delayed or non-pointing photons [16]. In addition, new dedicated experiments in the form of far detectors with a distance of $\sim 10 - 500$ meters away from the interaction points (IPs) have been under intensive discussion in the high-energy-physics community or even operated. For instance, FASER [17–19] is a relatively small and cheap cylindrical detector installed in the far forward direction of the ATLAS IP with a distance of 480 meter along the beam axis. It has been running and collecting data during the LHC Run 3 phase, with early results already published [20, 21]. Other proposals include MATHUSLA [7, 22, 23], MoEDAL-MAPP [24, 25], and CODEX-b [26, 27].

Typical NP candidates of LLPs include sterile neutrinos, dark Higgs, electroweakinos in supersymmetry (SUSY) models, dark photons, and axion-like particles (ALPs). Here, we focus on the ALPs and their phenomenology at the LHC (see for example Refs. [28–33] for some past studies in this direction). The ALPs are pseudoscalar particles predicted in many UV-complete BSM models such as string compactifications [34, 35], supersymmetry models [36], and Froggatt-Nielsen models of flavor [37, 38]. While they do not necessarily solve the strong CP problem in the SM as the QCD axions do with an extra $U(1)_{\text{PQ}}$ global symmetry breaking [39–41], their particular feature of having the ALP mass and the global symmetry breaking scale decoupled, allows for a rich phenomenology at various terrestrial experiments. More concretely, we consider a scenario with a Lagrangian where the ALPs couple to quarks only at tree level, both diagonally and off-diagonally leading to flavor-changing-neutral-current interactions. In particular, for the off-diagonal couplings, we restrict ourselves to those with the top quark and the up/charm quark. For the diagonal couplings, we include both up-type and down-type quarks in all generations. Phenomenological studies of quark-flavor-violating (QFV) ALPs can be found in e.g. Refs. [42–44]¹.

Owing to the large cross sections of the top-quark pair production at the LHC, we choose to study the rare decay of the top quarks into an ALP and an up/charm quark, with the ALP being long-lived and decaying hence with a displaced vertex (DV) dominantly into jets. While the signal process studied here is almost identical to that in Ref. [43], we approach the topic in a different manner. Specifically, since the considered signal process involves multiple jets from both the prompt decays of the top quarks and the displaced decay of the ALP, we recast a recent ATLAS search for the same signature [49] and thus reinterpret its exclusion bounds into the parameter space of the ALP model.

In Ref. [49], a “search for long-lived, massive particles in events with displaced vertices and multiple jets” was reported, at the center-of-mass (CM) energy $\sqrt{s} = 13$ TeV with 139 fb^{-1} integrated luminosity data collected during the LHC Run 2. Exclusion bounds were obtained at 95% C.L. on long-lived electroweakinos originating in either strong or electroweak (EW) production channels. Since the search required the LLP’s mass to be larger than 10 GeV, we will hence focus on the ALP mass range around [10, 100] GeV.

We now briefly discuss the current bounds on the ALPs coupled to quarks. The existing limits mainly stem from low-energy precision measurements or collider searches; see e.g. Refs. [42, 50]. The primary low-energy precision observables include rare decays of kaons, D - and B -mesons, and J/Ψ , and are, for phase-space reasons, relevant only to the ALPs lighter than the bottom mesons. For ALPs heavier than 10 GeV, collider searches have placed constraints. Firstly, Ref. [47] studies a theoretical scenario of the ALP coupled diagonally to a pair of top quarks only. It considers existing bounds on the coupling from various sources including low-energy precision measurements and collider searches. Specifically, for ALP mass $\gtrsim 10$ GeV, the strongest bounds are derived by recasting an ATLAS search [51] for “events with two opposite-charge leptons, jets and missing transverse momentum”, in terms of an ALP signal $pp \rightarrow t\bar{t}a$. These constraints are relevant to our study since we assume homogeneous flavor-diagonal couplings of the

¹See also Refs. [45–48] for studies on the ALPs coupled to the top quarks only.

ALPs to the quarks. However, as we will see later in the numerical results, the ATLAS search performed in Ref. [51] can, as shown in Ref. [47], constrain the effective coupling, for $m_a \sim [10, 100]$ GeV, orders of magnitude weaker than those probed in this work by the ATLAS search [49]. Second, Ref. [43] derives bounds on the ALP couplings to a top quark and an up/charm quark by a simple recast of a CMS search [52] mainly taking into account the ALP decay positions with exponential decay distributions, for the ALP masses of 2 and 10 GeV only. Therefore, we conclude that for the ALP mass range we study, current constraints on our model’s parameters, either are very weak, or stem potentially from other collider searches which we do not consider here.

This paper is organized as follows. In the next section we provide details of the model of the ALPs we consider, including the QFV terms. Expressions of the signal decay widths of the top quark and the ALP are also given, together with the signal process studied in this work. Then in Sec. 3, we describe the ATLAS search we recast, and elaborate on the simulation and computation procedures. The numerical results of the LHC exclusion bounds and the projected future high-luminosity LHC (HL-LHC) sensitivity reach are presented and discussed in Sec. 4. Finally, in Sec. 5, we summarize the work and provide an outlook. Additionally, in Appendix A, we detail the recasting procedure and results for the ATLAS DV+jets search.

2 The ALP model with quark flavor violation

We consider the following low-energy effective Lagrangian with ALP axial couplings to the quarks:

$$\begin{aligned} \mathcal{L}_{a, \text{eff}} = & \frac{\partial^\mu a}{2\Lambda} \left(\sum_{i=1,2,3} g_{ii} \bar{q}_i \gamma_\mu \gamma_5 q_i + \sum_{i,j=1,2,3}^{i \neq j} g_{ij} \bar{u}_i \gamma_\mu \gamma_5 u_j \right) \\ & + \frac{1}{2} (\partial_\mu a) (\partial^\mu a) - \frac{1}{2} m_a^2 a^2, \end{aligned} \quad (2.1)$$

where q_i labels either up-type or down-type quarks of generation indices i , and $u_{i,j}$ denotes the up-type quarks of generation i, j . We assume that the g couplings are real and positive, as well as symmetric in i, j such that $g_{ij} = g_{ji}$ for $i \neq j$. We do not include off-diagonal couplings for the down-type quarks in the theory. a denotes the ALP and Λ is the effective cutoff scale. For numerical studies, we implement our model with FeynRules [53, 54] in the UFO [55] format.

We study the following signal process,

$$pp \xrightarrow{\text{SM}} t\bar{t}, (t \rightarrow W^+ b, W^+ \rightarrow jj), (\bar{t} \rightarrow \bar{u}_i a, a \xrightarrow{\text{disp.}} jj), \text{ with } i = 1, 2, \quad (2.2)$$

and its charge-conjugated mode. jj denotes two jets including the b -quarks. In particular, the ALP here is long-lived and decays to two jets with a macroscopic displacement from the IP. For mediating the signal process, we assume all the diagonal couplings g_{ii} with $i = 1, 2, 3$, are non-vanishing and universal, and for the off-diagonal couplings, we consider only non-zero $g_{31} = g_{13} = g_{32} = g_{23}$ couplings for numerical studies.

The top-quark decay width into the ALP and an up-type quark u_i via g_{3i} is,

$$\Gamma(t \rightarrow au_i) = \frac{N_c}{384\pi} \frac{g_{3i}^2 m_a^2}{\Lambda^2 m_t} \left(\frac{(m_t^2 - m_{u_i}^2)^2}{m_a^2} - (m_t^2 + m_{u_i}^2) \right) \times \sqrt{\left(1 - \frac{(m_a + m_{u_i})^2}{m_t^2}\right) \left(1 - \frac{(m_a - m_{u_i})^2}{m_t^2}\right)}, \quad (2.3)$$

and the same contributions from g_{i3} are implied. Here, $N_c = 3$ is the number of QCD colors. We then obtain the corresponding top-quark decay branching ratio (BR) by considering the experimentally measured value of the top-quark total decay width, $\Gamma_t = 1.42$ GeV [56].

The ALP can decay to a pair of quarks with the same flavor $q_i \bar{q}_i$ via the diagonal couplings given in the Lagrangian, cf. Eq. (2.1), and the corresponding decay width is given below [48, 50]

$$\Gamma(a \rightarrow q_i \bar{q}_i) = \frac{N_c m_a m_{q_i}^2}{8\pi} \frac{g_{ii}^2}{\Lambda^2} \sqrt{1 - 4m_{q_i}^2/m_a^2}, \quad (2.4)$$

applicable in the regime of perturbative QCD ($m_a \gtrsim 1$ GeV). For ALP mass close to 100 GeV, the ALP decay BR into a pair of gluons via a triangle quark-loop with the same g_{ii} couplings can be up to about 40% [43], which is ignored for simplicity in this work.

Similarly, the ALP can decay to a pair of photons via a triangle quark-loop. We verified that for the $\mathcal{O}(10)$ GeV mass range of the ALP considered in this work, this loop-induced decay into two photons is suppressed by more than two orders of magnitude compared to that of the tree-level decay channel into a pair of quarks, and therefore we do not take into account this photon-pair channel in the numerical computation. In addition, we ignore the ALP decays into a pair of quarks via a triangle loop which includes two quarks and a W -boson.

The non-zero off-diagonal couplings lead to 3-body or 4-body ALP decays that can be important if the production couplings are orders of magnitude stronger than the decay couplings:

$$a \xrightarrow{g_{3i}} \bar{u}_i t^* \rightarrow \bar{u}_i b W^{+(*)} \rightarrow \bar{u}_i b (j j \text{ or } l^+ \nu), \quad \text{with } i = 1, 2, \quad (2.5)$$

and the charge-conjugate channel, where the W -boson can be either off-shell (4-body decays) or on-shell (3-body decays) depending on the ALP mass. For ALP mass below roughly $m_W + m_b \sim 85$ GeV, the off-diagonal production couplings g_{3i} can induce 4-body decays of the ALP which can be the dominant decay modes if the production coupling is larger than the decay coupling by at least around 4 orders of magnitude as we test with MadGraph5 [57, 58]; since the automatic calculation of the decay widths of these 4-body decay modes within MadGraph5 consumes too much computing resource, we do not include them in our computation and restrict ourselves to the parameter space where such contributions are unimportant. For ALP masses above the W -boson threshold, the non-diagonal couplings can result in 3-body decays of the ALP and these modes are taken into account in our computation. Moreover, flavor-diagonal ALP-quark couplings can also induce 4-body decays of the ALP, via an off-shell W -boson; however, these decay channels are always subdominant compared to the leading 2-body decays induced by the same couplings, and are hence ignored.

3 Experiment and simulation

3.1 The ATLAS DV+jets search

The ATLAS search [49] focused on the final-state signature of a DV plus multiple jets, with the proton-proton collision CM energy $\sqrt{s} = 13$ TeV and an integrated luminosity 139 fb^{-1} collected during the Run 2 phase of the LHC. The search employed two signal regions (SRs) called “High- p_T jet” and “Trackless jet”. Both SRs started with a certain but different set of selections on the numbers of jets with various p_T thresholds. This step accounts for the event-level acceptance. The two SRs then require that in the event there should be at least one vertex passing a list of vertex-level selections, including decaying inside the fiducial volume, having at least one displaced track with a transverse impact parameter larger than 2 mm, and DV invariant mass being larger than 10 GeV. For the events that have passed both event-level and vertex-level acceptances, parameterized efficiencies, provided by the ATLAS collaboration² to account for e.g. multi-jet trigger, high- p_T /trackless jet filter, and material effects in the High- p_T -jet and Trackless-jet SRs separately, are applied in order to attain the final cutflow.

The ATLAS search considered a benchmark case of long-lived electroweakinos in the R-parity-violating supersymmetry (RPV-SUSY), in which these electroweakinos decay into quarks via baryon-number-violating $\lambda'' \bar{U} \bar{D} \bar{D}$ operators. Two production channels of these electroweakinos are included. The first is via strong interaction where gluinos are pair produced, which subsequently decay to the lightest neutralinos and jets. The second is the direct electroweak production of a pair of electroweakinos including the lightest and the second lightest neutralinos as well as the lightest charginos.

We present the detail of the recasting procedures and validation results in Appendix A. In this recast, we compare our cutflow efficiencies step by step in various benchmarks with different masses of the gluino or electroweakinos, as well as the latter’s lifetimes, with those obtained with the ATLAS full simulation and with the ATLAS own recast. For all the benchmarks, we achieve $\mathcal{O}(1)\%$ level agreement with the experimental, published results at the cutflow steps of the event and vertex acceptances, while, when the parameterized efficiencies are included, in some benchmarks deviations (“non-closures”) as large as $\mathcal{O}(10)\%$ are observed.

3.2 Simulation and computation

With MadGraph5 [57, 58] and the UFO model that we have implemented, we generate one million signal events of the ALPs at the LHC (see Eq. (2.2)) at multiple parameter points in a grid scan covering the production couplings, decay couplings, as well as the ALP mass. The ALP decay width is automatically calculated within MadGraph5.

The generated signal-event files, in the LHEF [59] format, are then fed to Pythia8 [60] for showering, hadronization, and completing the truth-level decay chains of the various produced particles. With our recasting code (see Appendix A), we obtain the cutflow

²The relevant information including the materials for recasting can be found at the ATLAS HEPData webpage <https://www.hepdata.net/record/ins2628398>.

m_a [GeV], g_{ii}/Λ [GeV $^{-1}$], $c\tau_a$ [mm]	25, 10^{-9} , 2999	25, 10^{-8} , 29.99	25, 10^{-7} , 0.2999	40, 10^{-9} , 1790	40, 10^{-8} , 17.9	40, 10^{-7} , 0.179
Jet selection	9.9×10^{-4}	9.6×10^{-4}	1.0×10^{-3}	8.9×10^{-4}	8.9×10^{-4}	8.9×10^{-4}
Event has ≥ 1 DV passing:						
$R_{xy}, z < 300$ mm	1.8×10^{-5}	6.5×10^{-4}	1.0×10^{-3}	3.7×10^{-5}	8.0×10^{-4}	8.9×10^{-4}
$R_{xy} > 4$ mm	1.7×10^{-5}	6.2×10^{-4}	1.9×10^{-4}	3.7×10^{-5}	7.5×10^{-4}	3.6×10^{-5}
≥ 1 track with $ d_0 > 2$ mm	1.7×10^{-5}	6.1×10^{-4}	1.5×10^{-4}	3.7×10^{-5}	7.5×10^{-4}	2.9×10^{-5}
$n_{\text{selected decay products}} \geq 5$	1.3×10^{-5}	5.9×10^{-4}	1.4×10^{-4}	3.4×10^{-5}	7.3×10^{-4}	2.9×10^{-5}
Invariant mass > 10 GeV	7.0×10^{-6}	3.8×10^{-4}	1.1×10^{-4}	2.9×10^{-5}	6.6×10^{-4}	2.5×10^{-5}
Param. Effi.	2.3×10^{-8}	2.7×10^{-5}	2.3×10^{-5}	2.0×10^{-6}	1.2×10^{-4}	1.2×10^{-5}
m_a [GeV], g_{ii}/Λ [GeV $^{-1}$], $c\tau_a$ [mm]	65, 10^{-9} , 1080	65, 10^{-8} , 10.8	65, 10^{-7} , 0.108	90, 10^{-9} , 777	90, 10^{-8} , 7.77	90, 10^{-7} , 0.0777
Jet selection	1.0×10^{-3}	9.2×10^{-4}	9.8×10^{-4}	1.0×10^{-3}	9.5×10^{-4}	9.7×10^{-4}
Event has ≥ 1 DV passing:						
$R_{xy}, z < 300$ mm	8.4×10^{-5}	9.0×10^{-4}	9.8×10^{-4}	1.4×10^{-4}	9.4×10^{-4}	9.7×10^{-4}
$R_{xy} > 4$ mm	8.2×10^{-5}	7.5×10^{-4}	0.0	1.3×10^{-4}	7.3×10^{-4}	0.0
≥ 1 track with $ d_0 > 2$ mm	8.1×10^{-5}	7.5×10^{-4}	0.0	1.3×10^{-4}	7.2×10^{-4}	0.0
$n_{\text{selected decay products}} \geq 5$	8.0×10^{-5}	7.5×10^{-4}	0.0	1.3×10^{-4}	7.2×10^{-4}	0.0
Invariant mass > 10 GeV	7.9×10^{-5}	7.2×10^{-4}	0.0	1.3×10^{-4}	7.1×10^{-4}	0.0
Param. Effi.	1.3×10^{-5}	2.5×10^{-4}	0.0	2.8×10^{-5}	3.0×10^{-4}	0.0

Table 1. Cutflows on one million signal events with the High- p_T -jet search strategy for selected benchmark parameters of the ALP scenario, for $m_a = 25, 40, 65$, and 90 GeV, including the parameterized efficiencies. The ALP’s proper decay length, $c\tau_a$, is calculated with the given values of m_a and g_{ii}/Λ , with $g_{ii} = g_{11} = g_{22} = g_{33}$ and with Eq. (2.4). Note that we assume the production couplings are sufficiently small so that their induced partial decay widths are negligible; in practice, we fix $g_{3i}/\Lambda = 10^{-6}$ GeV $^{-1}$ for $i = 1, 2$ to obtain this table.

efficiencies ϵ for all the parameter points scanned. Thus, we compute the signal-event numbers with the following formula,

$$N_S = 2 \cdot \mathcal{L} \cdot \sigma(pp \rightarrow t\bar{t})_{\text{SM}} \cdot \mathcal{B}(t \rightarrow W^+b) \cdot \mathcal{B}(W^+ \rightarrow jj) \cdot \mathcal{B}(\bar{t} \rightarrow ja) \cdot \mathcal{B}(a \rightarrow jj) \cdot \epsilon, \quad (3.1)$$

where \mathcal{L} labels the integrated luminosity, $\mathcal{B}(t \rightarrow W^+b) = 99.7\%$, and $\mathcal{B}(W^+ \rightarrow jj) = 67.41\%$ [56]. Here “ j ” denotes a jet including the up, down, strange, charm, and bottom quarks. The theoretical prediction for the top-quark pair production cross section at the LHC $\sigma(pp \rightarrow t\bar{t})_{\text{SM}} = 833.9$ pb is computed at NNLO+NNLL with the Top++2.0 program, for the CM energy $\sqrt{s} = 13$ TeV [61].

4 Numerical results

In this section, we present and discuss the numerical results of our reinterpretation of the ATLAS DV+jets search [49] in terms of the QFV ALP scenario.

Reference [49] published in its Table 6 the observed limits at 95% C.L. on the signal-event number, $S_{\text{obs}}^{95} = 3.8(3.0)$ for the High- p_T (Trackless)-jet SR with an integrated luminosity of 139 fb $^{-1}$. We require these signal-event numbers for the ALP scenario in order to establish the corresponding exclusion bounds. Further, in expectation of advancement in e.g. technology and experimental search algorithms, we assume, for an integrated luminosity of 3000 fb $^{-1}$, the same level of background and hence the same number of expected signal-event numbers for the sensitivity reach at 95% C.L.

We first list the cutflows including the acceptances and the final parameterized efficiencies on one million signal events for selected example benchmark parameters of our signal

m_a [GeV], g_{ii}/Λ [GeV $^{-1}$], $c\tau_a$ [mm]	25, 10^{-9} , 2999	25, 10^{-8} , 29.99	25, 10^{-7} , 0.2999	40, 10^{-9} , 1790	40, 10^{-8} , 17.9	40, 10^{-7} , 0.179
Jet selection	3.1×10^{-3}	1.5×10^{-2}	1.5×10^{-2}	6.7×10^{-3}	1.5×10^{-2}	1.5×10^{-2}
Event has ≥ 1 DV passing:						
$R_{xy}, z < 300$ mm	2.3×10^{-4}	1.0×10^{-2}	1.5×10^{-2}	6.1×10^{-4}	1.3×10^{-2}	1.5×10^{-2}
$R_{xy} > 4$ mm	2.3×10^{-4}	9.7×10^{-3}	2.3×10^{-3}	6.0×10^{-4}	1.2×10^{-2}	2.9×10^{-4}
≥ 1 track with $ d_0 > 2$ mm	2.2×10^{-4}	9.6×10^{-3}	1.7×10^{-3}	6.0×10^{-4}	1.2×10^{-2}	2.3×10^{-4}
$n_{\text{selected decay products}} \geq 5$	2.1×10^{-4}	9.2×10^{-3}	1.7×10^{-3}	5.6×10^{-4}	1.2×10^{-2}	2.3×10^{-4}
Invariant mass > 10 GeV	1.3×10^{-4}	5.9×10^{-3}	1.2×10^{-3}	5.0×10^{-4}	1.1×10^{-2}	2.2×10^{-4}
Param. Effi.	6.8×10^{-6}	5.0×10^{-4}	2.4×10^{-4}	6.5×10^{-5}	2.3×10^{-3}	7.9×10^{-5}
m_a [GeV], g_{ii}/Λ [GeV $^{-1}$], $c\tau_a$ [mm]	65, 10^{-9} , 1080	65, 10^{-8} , 10.8	65, 10^{-7} , 0.108	90, 10^{-9} , 777	90, 10^{-8} , 7.77	90, 10^{-7} , 0.0777
Jet selection	1.3×10^{-2}	1.7×10^{-2}	1.7×10^{-2}	1.7×10^{-2}	1.8×10^{-2}	1.8×10^{-2}
Event has ≥ 1 DV passing:						
$R_{xy}, z < 300$ mm	1.6×10^{-3}	1.7×10^{-2}	1.7×10^{-2}	2.9×10^{-3}	1.8×10^{-2}	1.8×10^{-2}
$R_{xy} > 4$ mm	1.6×10^{-3}	1.4×10^{-2}	4.0×10^{-6}	2.9×10^{-3}	1.3×10^{-2}	0.0
≥ 1 track with $ d_0 > 2$ mm	1.6×10^{-3}	1.4×10^{-2}	3.0×10^{-6}	2.9×10^{-3}	1.3×10^{-2}	0.0
$n_{\text{selected decay products}} \geq 5$	1.6×10^{-3}	1.4×10^{-2}	3.0×10^{-6}	2.9×10^{-3}	1.3×10^{-2}	0.0
Invariant mass > 10 GeV	1.5×10^{-3}	1.3×10^{-2}	3.0×10^{-6}	2.8×10^{-3}	1.3×10^{-2}	0.0
Param. Effi.	2.7×10^{-4}	5.4×10^{-3}	1.2×10^{-6}	6.2×10^{-4}	6.8×10^{-3}	0.0

Table 2. The same table as Table 1, but for the Trackless-jet search strategy.

model in Table 1 and Table 2, for the High- p_T -jet SR and Trackless-jet SR, respectively. For $m_a = 25, 40, 65$, and 90 GeV, we consider the decay couplings $g_{ii}/\Lambda = 10^{-9}, 10^{-8}$, and 10^{-7} GeV $^{-1}$ and compute the corresponding proper decay length of the ALP, $c\tau_a$, collectively listed in the tables. In particular, for simplicity, we assume negligibly small production couplings so that their induced decays of the ALP can be safely neglected; specifically, we set $g_{3i}/\Lambda = 10^{-6}$ GeV $^{-1}$ with $i = 1, 2$ for deriving Table 1 and Table 2. We also note that, here, g_{ii} denotes the decay couplings $g_{11} = g_{22} = g_{33}$.

Now we present in Fig. 1 sensitivity reach of the ATLAS DV+jets search in the parameter plane $\frac{g_{31}}{\Lambda} = \frac{g_{32}}{\Lambda}$ vs. $\frac{g_{11}}{\Lambda} = \frac{g_{22}}{\Lambda} = \frac{g_{33}}{\Lambda}$, with the ALP mass fixed at 25, 40, 65, and 90 GeV.

The left(right) panel corresponds to the numerical results obtained with the ‘‘High p_T ’’ (‘‘Trackless’’) -jet search SR. Further, the solid and dashed lines are for an integrated luminosity of 139 fb $^{-1}$ and 3000 fb $^{-1}$, respectively. We apply a conservative 50% error band on these results arising from the uncertainties in the cutflow efficiencies, in particular, considering the non-closure we observe in our recast validation which can be up to about 75% in some benchmarks (see Appendix A), as well as from the uncertainties in our computation of the ALP’s decay widths. Note that the gray hatched region is where the 4-body decay widths of the ALP with a mass below about 85 GeV induced by the production couplings g_{31} and g_{32} , which we do not take into account in our numerical evaluation, are non-negligible, and hence also where our sensitivity reach is inaccurate.

In general we find that the two SRs are sensitive to similar decay-coupling ranges and hence similar lifetimes of the ALP. For the sensitivity reach in the production couplings, however, we observe that the Trackless-jet SR performs much better than the High- p_T -jet SR by a factor of ~ 5 . For the HL-LHC integrated luminosity of 3000 fb $^{-1}$ the sensitivity reach in the production couplings is stronger than that for the LHC Run 2 integrated luminosity of 139 fb $^{-1}$ by roughly ~ 5 ; this is because the signal-event number is proportional

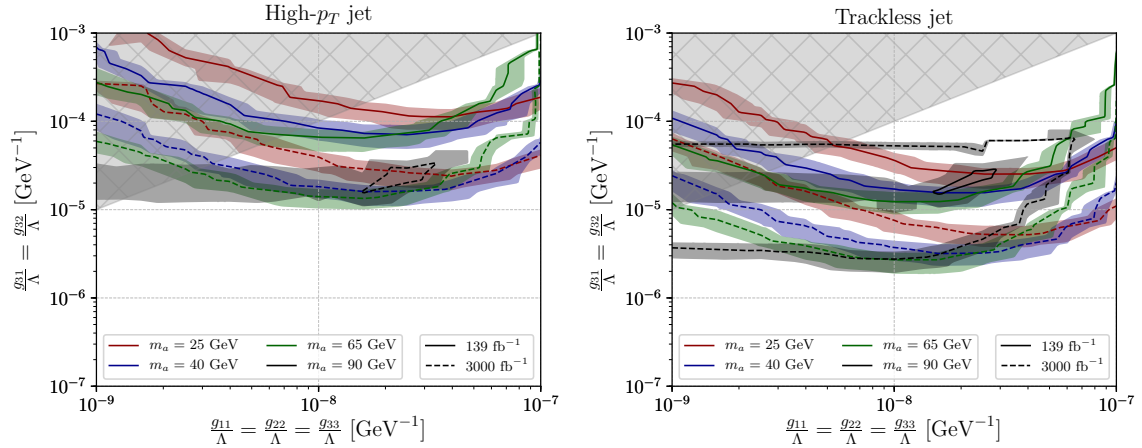


Figure 1. ATLAS sensitivity reach at 95% C.L. with 139 fb^{-1} (solid) and 3 ab^{-1} (dashed) integrated luminosities, in the plane $\frac{g_{31}}{\Lambda} = \frac{g_{32}}{\Lambda}$ vs. $\frac{g_{11}}{\Lambda} = \frac{g_{22}}{\Lambda} = \frac{g_{33}}{\Lambda}$, for various ALP mass choices, with the “High- p_T jet” (left) and “Trackless jet” (right) search strategies. An error band at 50% level is displayed together. The gray hatched region is where our results do not apply because we do not include the 4-body decay modes of the ALP induced by the production couplings for ALP masses below roughly 85 GeV. Bounds obtained in Ref. [47] by recasting the ATLAS search [51] is weak and outside the parameter range displayed here, and is hence not shown.

to the production couplings squared and thus re-scaling the integrated luminosities gives $\sqrt{3000/139} \sim 4.6$.

Both SRs show sensitivities to all the benchmark ALP masses studied, though the High- p_T -jet SR has no sensitivity to the case of $m_a = 90 \text{ GeV}$ with 139 fb^{-1} integrated luminosity. For $m_a = 90 \text{ GeV}$, the production couplings considered can lead to 3-body decays of the ALP into an up or charm quark, a W -boson, and a b -quark. Thus, the sensitivity reaches for $m_a = 90 \text{ GeV}$ are bounded from above.

Moving to Fig. 2, we show two plots in the plane $\frac{g_{ii}}{\Lambda} = \frac{1}{x} \frac{g_{31}}{\Lambda} = \frac{1}{x} \frac{g_{32}}{\Lambda}$ vs. m_a , for $x = 1000$ and 150 , respectively. In the left plot where the production couplings are assumed to be 1000 times the decay couplings, the High- p_T -jet SR is found to be sensitive only for $\mathcal{L} = 3000 \text{ fb}^{-1}$, while the Trackless-jet SR can probe the model for both 139 fb^{-1} and 3000 fb^{-1} integrated luminosities. We observe that for the ALP mass between about 12 GeV and 95 GeV, the Trackless-jet SR can probe the decay couplings g_{ii}/Λ , depending on the ALP mass, between about $3 \times 10^{-9} \text{ GeV}^{-1}$ and $5 \times 10^{-7} \text{ GeV}^{-1}$, for $\mathcal{L} = 3000 \text{ fb}^{-1}$. In the right plot, we assume smaller production couplings which are now 150 times the decay ones. This implies smaller production rates of the long-lived ALP, and, as a result, only the most sensitive SR, the Trackless-jet SR, with an integrated luminosity of 3000 fb^{-1} , would be sensitive to certain relatively small parts of the parameter space. Similar to Fig. 1, we assume an uncertainty level at 50% and show the corresponding error bands in these plots.

The sensitive regions are bounded from above; otherwise the decay widths would be too large for the ALP to decay inside the considered fiducial volume, which we define with some of the vertex-level acceptance selections: $R_{xy}, |z| < 300 \text{ mm}$ and $R_{xy} > 4 \text{ mm}$. For

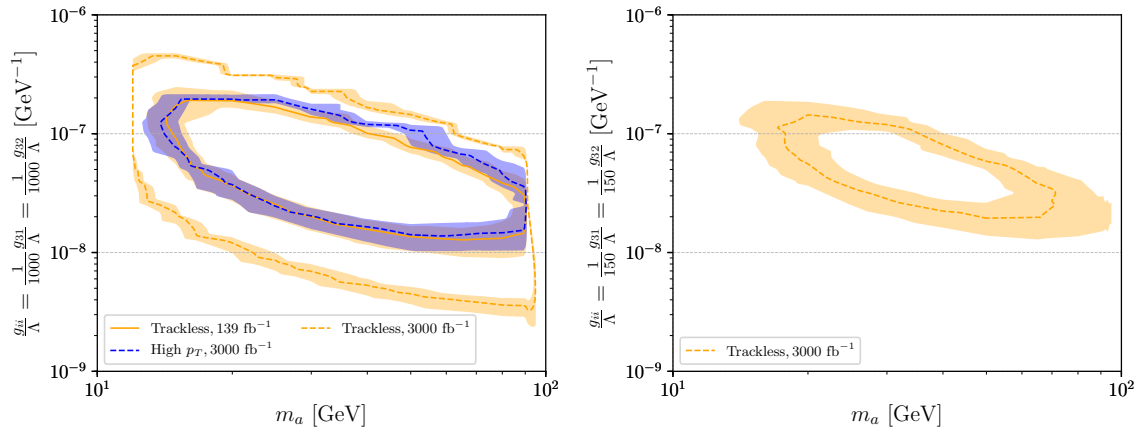


Figure 2. ATLAS sensitivity reach at 95% C.L. with 139 fb⁻¹ and 3 ab⁻¹ integrated luminosities, respectively, in the plane $\frac{g_{ii}}{\Lambda} = \frac{1}{x} \frac{g_{31}}{\Lambda} = \frac{1}{x} \frac{g_{32}}{\Lambda}$ vs. m_a for $x = 1000$ (left panel) and $x = 150$ (right panel), with the two search strategies. g_{ii} labels the universal quark-flavor-diagonal couplings with $g_{ii} = g_{11} = g_{22} = g_{33}$. As in Fig. 1, error bands at the level of 50% are shown.

the same reason, the sensitivity reach has an upper mass bound just below 100 GeV. The lower mass reach is mainly due to the invariant-mass requirement $m_{\text{DV}} > 10$ GeV in the vertex selections of the ATLAS search. Below the lower bounds of the sensitivity reach to the ALP couplings, the ALP production rates would be so small and the ALP decay length would be so long that the ALP tends to decay only after passing through the ATLAS detector’s fiducial volume, and these two effects combined lead to insufficient signal-event rates.

We further explain the overall slope of the ellipse-like sensitivity shape. This is mainly due to the effect of the ALP mass on the total decay width of the ALP, as generally speaking increasing the mass also enhances the total decay width. In the large-coupling regime, the ALP is rather prompt; as a result, with a larger m_a , the ALP becomes more prompt leading to even smaller decay probabilities of the ALP inside the fiducial volume. On the other hand, in the small-coupling limit, the ALP is already long-lived, where the signal-event rate is actually proportional to the ALP’s total decay width. This can be understood in the following way. The signal-event number is proportional to the decay probability of the ALP inside the fiducial volume, which can be computed with the exponential decay law, where the exponential functions can be expanded if the boosted decay length is much larger than the detector’s distance to the IP; as a result, the signal-event number would then be proportional to the ALP total decay width in the large decay-length, or equivalently, the small ALP-couplings limit. Therefore, as long as we are in this limit, a heavier ALP implies a larger decay width which then enhances the signal-event rates.

We note that the parameterized efficiencies provided by the ATLAS collaboration – while designed to be as model-independent as possible – were validated only for the RPV benchmarks tested by the collaboration, and therefore will have certain limitations when applied to other models. Nevertheless, as this is the public information we can access in

order to quantify the detector’s response to the displaced signal, we use these parameterized efficiencies while also discussing and checking these limitations’ relevance to our ALP scenarios before ending this section. The recasting instruction lists three conditions, under which the parameterized efficiencies are validated and hence recommended for use. Briefly summarized, these conditions require that:

1. the event- and vertex-level acceptances combined should exceed 10%;
2. for any parameter-space point, if the corresponding signal events have an acceptance of over 90% with the High- p_T -jet SR, the Trackless-jet SR should not be used; and
3. the LLP proper decay length of less than 3 meters are recommended for models where “jets primarily originate from the decay of LLPs”.

We examine our signal-event cutflows (see Table 1 and Table 2) closely against these conditions. Apparently, Condition 1 is not met in most, if not all, of the parameter-space points of the ALP scenario that we consider for both SRs. Consequently, Condition 2 is well satisfied. As for Condition 3, most of the parameter regions we study correspond to a $c\tau_a$ less than 3 meters; this can be confirmed easily if one observes, e.g. in Table 1, that for a relatively low mass $m_a = 25$ GeV and the minimal decay coupling over the effective scale we cover, 10^{-9} GeV $^{-1}$, $c\tau_a = 2.99$ m. Moreover, in our ALP model, jets stem not only from the ALP decays, but also, importantly, from the top quarks’ decays, and as a result, Condition 3 is not closely relevant for our study.

5 Summary and outlook

Recently, ATLAS published a search [49] for DV and multiple jets, obtaining latest bounds on electroweakinos in the RPV-SUSY which decay via baryon-number-violating operators $\lambda''\bar{U}\bar{D}\bar{D}$. The search has two SRs, High- p_T jet and Trackless jet, and both strong and electroweak production channels of the electroweakinos are considered in the ATLAS search. In this work, we have recast this search and validated our code by comparing cutflow efficiencies. We achieve excellent agreement at the acceptance level. However, once the parameterized efficiencies, provided by the ATLAS collaboration to account for further selections such as multi-jet trigger and detector material map, are included, we find good agreement only in some benchmarks while in other benchmarks our results can be off from the experimental full simulation by up to about 75%.

We then proceed to apply our recasting code in a theoretical scenario with an ALP coupled both diagonally and off-diagonally to quarks. Specifically, we focus on QFV couplings of the ALP with the top quark and the up/charm quark, primarily mediating the production of the ALP from top-quark decays. The diagonal couplings mainly lead to the tree-level decays of the ALP into jets. The ALP can be long-lived for sufficiently small couplings to the quarks, thus potentially forming a DV inside the fiducial volume (tracker) of the ATLAS detector. With our recasting code, we obtain the cutflow efficiencies at each scanned parameter point of the model, and then compute the expected signal-event

numbers with either the current 139 fb^{-1} or the future HL-LHC 3000 fb^{-1} integrated luminosity. This allows for obtaining the exclusion bounds at 95% C.L. We show our numerical results of the sensitivity reach in two figures. First, we fix the ALP mass at some representative values, and present the bounds in the plane of the production couplings vs. the decay couplings. We find both SRs are sensitive to certain parts of the parameter points, and the Trackless-jet SR performs better than the High- p_T -jet SR. In particular, for 139 fb^{-1} , the Trackless-jet SR can probe the ALP parameter space for the ALP mass even above the threshold of $m_W + m_b \sim 85 \text{ GeV}$, touching a unique part of the parameter space. We then fix the proportionality relations between the production and the decay couplings, and present sensitivity reach in the plane of the decay coupling vs. the ALP mass. We find the search with either 139 fb^{-1} or 3000 fb^{-1} integrated luminosity can be sensitive to the decay couplings $\frac{g_{ii}}{\Lambda}$ of order $\mathcal{O}(10^{-9}) - \mathcal{O}(10^{-7}) \text{ GeV}^{-1}$, for the ALP mass roughly between 12 GeV and 95 GeV and the production couplings being 1000 times the decay ones. For another benchmark where the production couplings are 150 times the decay ones, more restricted sensitivities are found. In addition, in Table 1 and Table 2 we list cutflows for representative mass and decay couplings of the ALP.

We conclude that the ATLAS search can probe unique parts of the parameter space of the QFV ALP scenario considered here, which are current not excluded. This sheds light on potential further applications of the search in other theoretical scenarios predicting DV plus jets.

Acknowledgment

We thank David Rousso, Emily Thompson, and Catherine Xu, for useful discussions concerning the recast of the ATLAS DV+jets search. We thank Jong Soo Kim and Kechen Wang for help with the jet merging procedure. G.C. acknowledges support from ANID FONDECYT grant No. 11220237 and ANID – Millennium Science Initiative Program ICN2019_044. The work was supported by the MoST of Taiwan under Grants MOST-110-2112-M-007-017-MY3.

A Recast of the DV+jets search

With MadGraph5 3.4.1 [57, 58], we generate signal-event sample LHE files in the theoretical framework of the MSSM. The SUSY SLHA spectrum files are provided by the ATLAS collaboration, where we only need to tune the gluino mass, electroweakinos' masses, as well as the total decay width of the electroweakinos according to the selected benchmarks given in Ref. [49]. All the other SUSY particles' masses have been set to very large decoupled values. For the strong-production channel, we simulate $pp \rightarrow \tilde{g}\tilde{g}$ events at the CM energy $\sqrt{s} = 13 \text{ TeV}$, where the gluinos decay promptly to the lightest neutralino (which is mainly bino-like) and two light jets with equal branching ratios shared between the down, up, strange, and charm quarks: $\tilde{g} \rightarrow \tilde{\chi}_1^0 jj$, and the lightest neutralino is set to decay to three light quarks via $\lambda'' \bar{U} \bar{D} \bar{D}$ operators. For the EW-production channels, pair-production processes of the mass-degenerate electroweakinos $\tilde{\chi}_1^0, \tilde{\chi}_2^0$, and $\tilde{\chi}_1^\pm$ are taken into account:

SR	High- p_T jet	Trackless jet
Jet selection	$n_{\text{jet}}^{250} \geq 4$ or $n_{\text{jet}}^{195} \geq 5$ or $n_{\text{jet}}^{116} \geq 6$ or $n_{\text{jet}}^{90} \geq 7$	$n_{\text{jet}}^{137} \geq 4$ or $n_{\text{jet}}^{101} \geq 5$ or $n_{\text{jet}}^{83} \geq 6$ or $n_{\text{jet}}^{55} \geq 7$, $n_{\text{displaced jet}}^{70} \geq 1$ or $n_{\text{displaced jet}}^{50} \geq 2$

Table 3. Truth-jet selection requirements. $n_{\text{jet}}^{250} \geq 4$ means at least 4 jets should have a p_T larger than or equal to 250 GeV, and similarly for the other notations.

$pp \rightarrow \tilde{\chi}_1^0 \tilde{\chi}_1^+, \tilde{\chi}_1^0 \tilde{\chi}_1^-, \tilde{\chi}_1^- \tilde{\chi}_1^+, \tilde{\chi}_1^0 \tilde{\chi}_2^0, \tilde{\chi}_2^0 \tilde{\chi}_1^+, \tilde{\chi}_2^0 \tilde{\chi}_1^-$. The electroweakinos, which are assumed to be pure Higgsinos, are then set to decay to either light or heavy quarks according to the benchmarks studied on hand.

The hard-process events are simulated together with up to two additional jets. We perform the CKKW-L jet merging scheme [62], setting in the `run_card.dat` of MadGraph5 that the value of `ktdurham` should be equal to the jet merging scale, which is a quarter of the gluino mass in the strong-channel processes and a quarter of the electroweakino masses in the EW processes. The generated LHE files are then showered and hadronized in Pythia8.308 [60] where we switch on `kT` merging with the jet-merging scale set to a quarter of the SUSY particles produced (equal to the value of `ktdurham` set in the `run_card.dat` of MadGraph5). It is important that we switch on `Merging:mayRemoveDecayProducts` in order to perform merging before the decay products of the resonances are generated in Pythia.

Note that during the event generation, `NNPDF2.31o` [63] is chosen for the parton distribution function of the protons, with the `A14` [64] tune.

Pre-selections: the default parton-level selections in MadGraph5 are used. We implement a toy-detector module in Pythia for reconstructing truth-level jets, in a similar way as in Ref. [65] but matching the truth-level selection for jets described in the HEPData recast instruction note for the DV+jets ATLAS search [49].

Truth jets are reconstructed with FastJet [66], using anti- k_t algorithm and $R = 0.4$ from all selected stable particles excluding neutrinos and muons. This definition includes particles from the LLP decay. Jet momentum smearing is applied with formulas given in Ref. [65]. Further, displaced jets are defined as those among the jets selected above that are matched with the LLPs' decay positions and have $|\eta| < 2.5$. By calculating ΔR between the LLP decay products and the truth jets, we determine that a truth jet stems from the LLP decay if the closest decay products of the LLP has $\Delta R < 0.3$. Furthermore, for the displaced truth jets, we require that the matched LLPs should decay with a transverse distance from IP smaller than 3870 mm which corresponds to the region of the calorimeter.

Event selections: we follow step-by-step the recasting instruction provided on HEPData by the ATLAS collaboration for this search. Event-level requirement of certain numbers of jets with different p_T thresholds is first applied onto the events. The detailed selections differ between the High- p_T -jet and the Trackless-jet SRs. We reproduce these requirements from Ref. [49] here in Table 3. For the events passing the jet selections, at least one vertex should pass a list of vertex requirements, in order to obtain the vertex-level

acceptance:

1. Both the transverse distance R_{xy} and the absolute longitudinal distance $|z|$ of the vertex from the IP should be smaller than 300 mm.
2. R_{xy} should further be larger than 4 mm.
3. At least one track should have a transverse impact parameter satisfying $d_0 > 2$ mm.
4. The displaced vertex should have at least 5 decay products of a massive particle satisfying the following requirements (“selected decay products”):
 - (a) It should be a track with a boosted transverse decay length larger than 520 mm.
 - (b) Its p_T and charge q should obey the relation $p_T/|q| > 1$ GeV.
5. The truth vertex should have an invariant mass larger than 10 GeV, which is constructed with the decay products passing the above requirements, for which the mass of each decay product is assumed to be that of a charged pion.

For events that have passed the above event and vertex acceptance requirements, we make use of parameterized efficiencies provided by the ATLAS collaboration at both event and vertex levels that account for quality requirements such as multi-jet trigger and material veto that are difficult to simulate. The event-level efficiencies ϵ_{event} are functions of the truth-jet scalar p_T sum and the transverse distance of the furthest LLP decay. The vertex-level efficiencies ϵ_{vertex} are for reconstructing the DVs, and are functions of the DV’s transverse distance to the IP, its invariant mass, as well as the LLP decay product multiplicity.

We compute the final cutflow efficiency with the following formula,

$$\epsilon = \mathcal{A}_{\text{event}} \cdot \epsilon_{\text{event}} \cdot \left(1 - \prod_{\text{vertex}} (1 - \mathcal{A}_{\text{vertex}} \cdot \epsilon_{\text{vertex}})\right), \quad (\text{A.1})$$

where $\mathcal{A}_{\text{event}}$ and $\mathcal{A}_{\text{vertex}}$ label the portion of events satisfying the event-level and vertex-level acceptance requirements, respectively.

In the following, we show tables listing the cutflow efficiency results’ comparison, considering both strong-channel and EW-channel benchmarks given in the recasting instruction; this includes not only light-flavor cases where the long-lived electroweakinos decay to light quarks, but also heavy-flavor ones. The heavy-flavor benchmarks are included for recasting validation, because in the ALP scenario we study, the long-lived ALP also decays to b -quarks.

In Table 4, we compare the full cutflow with acceptances only, for the High- p_T -jet SR in the strong-channel production of the lightest neutralinos which decay to light-flavor quarks. We find in all four benchmarks, the validation works very well in each step of the event-level and vertex-level acceptance selections.

In Table 5, we show results where now the parameterized efficiencies have been included in the computation. We compare the results of the experimental full simulation, recast results with the parameterized efficiencies given by the ATLAS collaboration, as well as

$m(\tilde{g})$ [GeV] $m(\tilde{\chi}_1^0)$ [GeV] $\tau(\tilde{\chi}_1^0)$ [ns]	Acceptance [%]							
	2000		2000		2400		2000	
	850		50		200		1250	
	0.01		0.1		1		10	
Selection	Exp.	This work	Exp.	This work	Exp.	This work	Exp.	This work
Jet selection	99.9	99.8	96.6	96.9	97.2	98.2	96.1	99.9
Event has ≥ 1 DV passing:								
$R_{xy}, z < 300$ mm	99.9	99.8	78.7	79.7	44.7	45.5	31.7	31.2
$R_{xy} > 4$ mm	29.6	29.7	77.0	78.3	43.8	44.7	30.9	30.5
≥ 1 track with $ d_0 > 2$ mm	29.6	29.7	75.6	77.6	43.7	44.7	30.9	30.5
$n_{\text{selected decay products}} \geq 5$	29.6	29.7	75.5	77.3	43.7	44.7	30.9	30.5
Invariant mass > 10 GeV	29.6	29.7	74.7	75.8	43.7	44.7	30.9	30.5

Table 4. High- p_T -jet SR acceptance with full cutflow. With the strong-channel production and the lightest neutralino decaying to light-flavor quarks.

$m(\tilde{g}), m(\tilde{\chi}_1^0), \tau(\tilde{\chi}_1^0)$	Full Sim.	Param. Exp.	Param. Ours	Non-closure
2000 GeV, 850 GeV, 0.01 ns	27.8%	26.0%	26.6%	-4.3%
2000 GeV, 50 GeV, 0.1 ns	14.4%	13.8%	21.6%	50.0%
2400 GeV, 200 GeV, 1 ns	11.5%	11.5%	14.4%	25.2%
2000 GeV, 1250 GeV, 10 ns	9.2%	8.6%	8.4%	-8.7%

Table 5. High- p_T -jet SR ϵ including both the acceptances’ and the parameterized efficiencies’ effects. With the strong-channel production and the lightest neutralino decaying to light-flavor quarks.

$m(\tilde{\chi}_1^0)$ [GeV] $\tau(\tilde{\chi}_1^0)$ [ns]	Acceptance [%]							
	500		500		1300		1300	
	0.1		1		0.1		1	
Selection	Exp.	This work	Exp.	This work	Exp.	This work	Exp.	This work
Jet selection	49.5	51.0	50.1	51.0	96.8	98.5	98.5	98.5
Event has ≥ 1 DV passing:								
$R_{xy}, z < 300$ mm	49.5	51.0	41.0	41.5	96.8	98.5	92.1	92.4
$R_{xy} > 4$ mm	46.5	47.6	39.8	40.4	85.9	86.9	89.9	90.5
≥ 1 track with $ d_0 > 2$ mm	46.5	47.6	39.8	40.4	85.9	86.9	89.9	90.5
$n_{\text{selected decay products}} \geq 5$	46.5	47.6	39.8	40.4	85.9	86.9	89.9	90.5
Invariant mass > 10 GeV	46.5	47.6	39.8	40.4	85.9	86.9	89.9	90.5

Table 6. Trackless-jet SR acceptance with full cutflow. With the EW-channel production and the electroweakinos decaying to light-flavor quarks.

our own recast results with the parameterized efficiencies. The final column “Non-closure” is defined as the difference between the full-simulation results and our recast results with respect to the full-simulation results, given in percentage. We observe that our recast is validated well in the first and the fourth benchmarks, while for the second and third benchmarks, non-closure is about 50% and 30%, respectively.

$m(\tilde{\chi}_1^0), \tau(\tilde{\chi}_1^0)$	Full Sim.	Param. Exp.	Param. Ours	Non-closure
500 GeV, 0.1 ns	31.1%	28.1%	34.6%	11.3%
500 GeV, 1 ns	14.3%	14.3%	24.9%	74.1%
1300 GeV, 0.1 ns	12.2%	11.7%	11.1%	-9.0%
1300 GeV, 1 ns	8.3%	7.9%	11.7%	41.0%

Table 7. Trackless-jet SR ϵ including including both the acceptances’ and the parameterized efficiencies’ effects. With the EW-channel production and the electroweakinos decaying to light-flavor quarks.

$m(\tilde{\chi}_1^0)$ [GeV] $\tau(\tilde{\chi}_1^0)$ [ns]	Acceptance [%]					
	1500 0.032		1500 0.1		1500 1	
Selection	Exp.	This work	Exp.	This work	Exp.	This work
Jet selection	84.7	82.5	84.7	82.4	84.7	82.4
Event has ≥ 1 DV passing:						
$R_{xy}, z < 300$ mm	84.7	82.5	84.7	82.4	80.1	78.0
$R_{xy} > 4$ mm	45.7	46.9	73.3	72.3	78.4	76.5
≥ 1 track with $ d_0 > 2$ mm	45.7	46.9	73.3	72.3	78.4	76.5
$n_{\text{selected decay products}} \geq 5$	45.7	46.9	73.3	72.3	78.4	76.5
Invariant mass > 10 GeV	45.7	46.9	73.3	72.3	78.4	76.5

Table 8. High- p_T -jet SR acceptance with full cutflow. With the EW-channel production and the electroweakinos decaying to heavy-flavor quarks. Note that for this scenario, the EW-production channel, instead of the strong channel, is considered, following the recasting material of Ref. [49].

$m(\tilde{\chi}_1^0), \tau(\tilde{\chi}_1^0)$	Full Sim.	Param. Exp.	Param. Ours	Non-closure
1500 GeV, 0.032 ns	39.6%	42.7%	45.6%	15.2%
1500 GeV, 0.1 ns	57.7%	62.7%	68.9%	19.4%
1500 GeV, 1 ns	36.7%	43.0%	65.0%	77.1%

Table 9. High- p_T -jet SR ϵ including both the acceptances’ and the parameterized efficiencies’ effects. With the EW-channel production and the electroweakinos decaying to heavy-flavor quarks.

Similarly, we show in Table 6 and Table 7 the validation results for the Trackless-jet SR in the EW-production channel of the electroweakinos decaying to light-flavor quarks. We come to similar conclusions that while for the acceptance cutflows we achieve very good validation, once the parameterized efficiencies are taken into account, only some benchmarks are well validated and the others show non-closure values up to about 70%.

Moving to the benchmarks where the electroweakinos decay to heavy-flavor quarks, we present in Table 8, Table 9, Table 10, and Table 11, the corresponding validation results. Here, only the EW-production channels are considered, and both the High- p_T -jet and

$m(\tilde{\chi}_1^0)$ [GeV] $\tau(\tilde{\chi}_1^0)$ [ns]	Acceptance [%]					
	700 0.032		700 0.1		700 1	
Selection	Exp.	This work	Exp.	This work	Exp.	This work
Jet selection	69.8	72.2	74.1	72.2	74.7	71.9
Event has ≥ 1 DV passing:						
$R_{xy}, z < 300$ mm	69.8	72.2	74.1	72.2	64.8	62.4
$R_{xy} > 4$ mm	48.4	48.5	68.1	66.3	62.9	60.9
≥ 1 track with $ d_0 > 2$ mm	48.4	48.5	68.1	66.3	62.9	60.9
$n_{\text{selected decay products}} \geq 5$	48.4	48.5	68.1	66.3	62.9	60.9
Invariant mass > 10 GeV	48.4	48.5	68.1	66.3	62.9	60.9

Table 10. Trackless-jet SR acceptance with full cutflow. With the EW-channel production and the electroweakinos decaying to heavy-flavor quarks.

$m(\tilde{\chi}_1^0), \tau(\tilde{\chi}_1^0)$	Full Sim.	Param. Exp.	Param. Ours	Non-closure
700 GeV, 0.032 ns	26.6%	28.2%	30.0%	12.8%
700 GeV, 0.1 ns	37.5%	36.7%	42.5%	13.3%
700 GeV, 1 ns	20.0%	21.1%	34.9%	74.5%

Table 11. Trackless-jet SR ϵ including both the acceptances' and the parameterized efficiencies' effects. With the EW-channel production and the electroweakinos decaying to heavy-flavor quarks.

Trackless-jet SRs are applied. We reach a similar conclusion as in the previous benchmarks, that the acceptance-only cutflows agree very well with the experimental published results, but with the inclusion of the parameterized efficiencies we find relatively unsatisfactory comparisons with large non-closure values in some benchmarks.

Given the generally excellent validation results with the acceptance requirements only, we argue that we should have selected the correct set of events from the whole event samples. Moreover, the event-level and vertex-level efficiencies are functions with input parameters that determine the acceptance-level cutflows. Therefore, after excluding possible issues within coding itself, we do not find an explanation for the discrepancies observed once the parameterized efficiencies are included, and thus urge for further collaboration between the theorists and experimentalists in order to resolve the issue. To aid this end, we have uploaded our code to the public LLP Recasting Repository [67], hoping it would be useful for other groups.

References

- [1] **ATLAS** Collaboration, G. Aad et al., *Observation of a new particle in the search for the Standard Model Higgs boson with the ATLAS detector at the LHC*, *Phys. Lett. B* **716** (2012) 1–29, [[arXiv:1207.7214](https://arxiv.org/abs/1207.7214)].

- [2] **CMS** Collaboration, S. Chatrchyan et al., *Observation of a New Boson at a Mass of 125 GeV with the CMS Experiment at the LHC*, *Phys. Lett. B* **716** (2012) 30–61, [[arXiv:1207.7235](#)].
- [3] P. Agrawal et al., *Feebly-interacting particles: FIPs 2020 workshop report*, *Eur. Phys. J. C* **81** (2021), no. 11 1015, [[arXiv:2102.12143](#)].
- [4] C. Antel et al., *Feebly Interacting Particles: FIPs 2022 workshop report*, *Eur. Phys. J. C* **83** (2023) 1122, [[arXiv:2305.01715](#)].
- [5] J. Alimena et al., *Searching for long-lived particles beyond the Standard Model at the Large Hadron Collider*, *J. Phys. G* **47** (2020), no. 9 090501, [[arXiv:1903.04497](#)].
- [6] L. Lee, C. Ohm, A. Soffer, and T.-T. Yu, *Collider Searches for Long-Lived Particles Beyond the Standard Model*, *Prog. Part. Nucl. Phys.* **106** (2019) 210–255, [[arXiv:1810.12602](#)]. [Erratum: *Prog.Part.Nucl.Phys.* 122, 103912 (2022)].
- [7] D. Curtin et al., *Long-Lived Particles at the Energy Frontier: The MATHUSLA Physics Case*, *Rept. Prog. Phys.* **82** (2019), no. 11 116201, [[arXiv:1806.07396](#)].
- [8] J. Beacham et al., *Physics Beyond Colliders at CERN: Beyond the Standard Model Working Group Report*, *J. Phys. G* **47** (2020), no. 1 010501, [[arXiv:1901.09966](#)].
- [9] **CMS** Collaboration, A. Hayrapetyan et al., *Search for supersymmetry in final states with disappearing tracks in proton-proton collisions at $\sqrt{s} = 13$ TeV*, [arXiv:2309.16823](#).
- [10] **ATLAS** Collaboration, G. Aad et al., *Search for long-lived charginos based on a disappearing-track signature using 136 fb^{-1} of pp collisions at $\sqrt{s} = 13$ TeV with the ATLAS detector*, *Eur. Phys. J. C* **82** (2022), no. 7 606, [[arXiv:2201.02472](#)].
- [11] **CMS** Collaboration, A. Hayrapetyan et al., *Search for long-lived particles using displaced vertices and missing transverse momentum in proton-proton collisions at $\sqrt{s} = 13$ TeV*, [arXiv:2402.15804](#).
- [12] **ATLAS** Collaboration, M. Aaboud et al., *Search for long-lived, massive particles in events with displaced vertices and missing transverse momentum in $\sqrt{s} = 13$ TeV pp collisions with the ATLAS detector*, *Phys. Rev. D* **97** (2018), no. 5 052012, [[arXiv:1710.04901](#)].
- [13] **ATLAS** Collaboration, G. Aad et al., *Search for long-lived, massive particles in events with a displaced vertex and a muon with large impact parameter in pp collisions at $\sqrt{s} = 13$ TeV with the ATLAS detector*, *Phys. Rev. D* **102** (2020), no. 3 032006, [[arXiv:2003.11956](#)].
- [14] **ATLAS** Collaboration, G. Aad et al., *Search for Displaced Leptons in $\sqrt{s} = 13$ TeV pp Collisions with the ATLAS Detector*, *Phys. Rev. Lett.* **127** (2021), no. 5 051802, [[arXiv:2011.07812](#)].
- [15] **CMS** Collaboration, A. Tumasyan et al., *Search for long-lived particles decaying to leptons with large impact parameter in proton–proton collisions at $\sqrt{s} = 13$ TeV*, *Eur. Phys. J. C* **82** (2022), no. 2 153, [[arXiv:2110.04809](#)].
- [16] **ATLAS** Collaboration, G. Aad et al., *Search for displaced photons produced in exotic decays of the Higgs boson using 13 TeV pp collisions with the ATLAS detector*, *Phys. Rev. D* **108** (2023), no. 3 032016, [[arXiv:2209.01029](#)].
- [17] J. L. Feng, I. Galon, F. Kling, and S. Trojanowski, *ForwArd Search ExpeRiment at the LHC*, *Phys. Rev. D* **97** (2018), no. 3 035001, [[arXiv:1708.09389](#)].

- [18] **FASER** Collaboration, A. Ariga et al., *FASER’s physics reach for long-lived particles*, *Phys. Rev. D* **99** (2019), no. 9 095011, [[arXiv:1811.12522](#)].
- [19] J. L. Feng et al., *The Forward Physics Facility at the High-Luminosity LHC*, *J. Phys. G* **50** (2023), no. 3 030501, [[arXiv:2203.05090](#)].
- [20] **FASER** Collaboration, H. Abreu et al., *First Direct Observation of Collider Neutrinos with FASER at the LHC*, *Phys. Rev. Lett.* **131** (2023), no. 3 031801, [[arXiv:2303.14185](#)].
- [21] **FASER** Collaboration, H. Abreu et al., *Search for dark photons with the FASER detector at the LHC*, *Phys. Lett. B* **848** (2024) 138378, [[arXiv:2308.05587](#)].
- [22] J. P. Chou, D. Curtin, and H. Lubatti, *New Detectors to Explore the Lifetime Frontier*, *Phys. Lett. B* **767** (2017) 29–36, [[arXiv:1606.06298](#)].
- [23] **MATHUSLA** Collaboration, C. Alpigiani et al., *An Update to the Letter of Intent for MATHUSLA: Search for Long-Lived Particles at the HL-LHC*, [arXiv:2009.01693](#).
- [24] J. L. Pinfold, *The MoEDAL experiment: a new light on the high-energy frontier*, *Phil. Trans. Roy. Soc. Lond. A* **377** (2019), no. 2161 20190382.
- [25] J. L. Pinfold, *The MoEDAL Experiment at the LHC—A Progress Report*, *Universe* **5** (2019), no. 2 47.
- [26] V. V. Gligorov, S. Knapen, M. Papucci, and D. J. Robinson, *Searching for Long-lived Particles: A Compact Detector for Exotics at LHCb*, *Phys. Rev. D* **97** (2018), no. 1 015023, [[arXiv:1708.09395](#)].
- [27] G. Aielli et al., *Expression of interest for the CODEX-b detector*, *Eur. Phys. J. C* **80** (2020), no. 12 1177, [[arXiv:1911.00481](#)].
- [28] M. Bauer, M. Neubert, and A. Thamm, *Collider Probes of Axion-Like Particles*, *JHEP* **12** (2017) 044, [[arXiv:1708.00443](#)].
- [29] G. Alonso-Álvarez, J. Jaeckel, and D. D. Lopes, *Tracking axion-like particles at the LHC*, [arXiv:2302.12262](#).
- [30] J. Ren, D. Wang, L. Wu, J. M. Yang, and M. Zhang, *Detecting an axion-like particle with machine learning at the LHC*, *JHEP* **11** (2021) 138, [[arXiv:2106.07018](#)].
- [31] F. A. Ghebretinsaea, Z. S. Wang, and K. Wang, *Probing axion-like particles coupling to gluons at the LHC*, *JHEP* **07** (2022) 070, [[arXiv:2203.01734](#)].
- [32] C. Baldenegro, S. Hassani, C. Royon, and L. Schoeffel, *Extending the constraint for axion-like particles as resonances at the LHC and laser beam experiments*, *Phys. Lett. B* **795** (2019) 339–345, [[arXiv:1903.04151](#)].
- [33] A. Flórez, A. Gurrola, W. Johns, P. Sheldon, E. Sheridan, K. Sinha, and B. Soubasis, *Probing axionlike particles with $\gamma\gamma$ final states from vector boson fusion processes at the LHC*, *Phys. Rev. D* **103** (2021), no. 9 095001, [[arXiv:2101.11119](#)].
- [34] M. Cicoli, *Axion-like Particles from String Compactifications*, in *9th Patras Workshop on Axions, WIMPs and WISPs*, pp. 235–242, 2013. [arXiv:1309.6988](#).
- [35] A. Ringwald, *Searching for axions and ALPs from string theory*, *J. Phys. Conf. Ser.* **485** (2014) 012013, [[arXiv:1209.2299](#)].
- [36] B. Bellazzini, A. Mariotti, D. Redigolo, F. Sala, and J. Serra, *R-axion at colliders*, *Phys. Rev. Lett.* **119** (2017), no. 14 141804, [[arXiv:1702.02152](#)].

- [37] C. D. Froggatt and H. B. Nielsen, *Hierarchy of Quark Masses, Cabibbo Angles and CP Violation*, *Nucl. Phys. B* **147** (1979) 277–298.
- [38] T. Alanne, S. Blasi, and F. Goertz, *Common source for scalars: Flavored axion-Higgs unification*, *Phys. Rev. D* **99** (2019), no. 1 015028, [[arXiv:1807.10156](#)].
- [39] R. D. Peccei and H. R. Quinn, *CP Conservation in the Presence of Instantons*, *Phys. Rev. Lett.* **38** (1977) 1440–1443.
- [40] R. D. Peccei and H. R. Quinn, *Constraints Imposed by CP Conservation in the Presence of Instantons*, *Phys. Rev. D* **16** (1977) 1791–1797.
- [41] F. Wilczek, *Problem of Strong P and T Invariance in the Presence of Instantons*, *Phys. Rev. Lett.* **40** (1978) 279–282.
- [42] A. Carmona, C. Scherb, and P. Schwaller, *Charming ALPs*, *JHEP* **08** (2021) 121, [[arXiv:2101.07803](#)].
- [43] A. Carmona, F. Elahi, C. Scherb, and P. Schwaller, *The ALPs from the top: searching for long lived axion-like particles from exotic top decays*, *JHEP* **07** (2022) 122, [[arXiv:2202.09371](#)].
- [44] T. Li, Z. Qian, M. A. Schmidt, and M. Yuan, *The quark flavor-violating ALPs in light of B mesons and hadron colliders*, [arXiv:2402.14232](#).
- [45] S. Blasi, F. Maltoni, A. Mariotti, K. Mimasu, D. Pagani, and S. Tentori, *Top-philic ALP phenomenology at the LHC: the elusive mass-window*, [arXiv:2311.16048](#).
- [46] A. V. Phan and S. Westhoff, *Precise tests of the axion coupling to tops*, [arXiv:2312.00872](#).
- [47] F. Esser, M. Madigan, V. Sanz, and M. Ubiali, *On the coupling of axion-like particles to the top quark*, *JHEP* **09** (2023) 063, [[arXiv:2303.17634](#)].
- [48] L. Rygaard, J. Niedziela, R. Schäfer, S. Bruggisser, J. Alimena, S. Westhoff, and F. Blekman, *Top Secrets: long-lived ALPs in top production*, *JHEP* **10** (2023) 138, [[arXiv:2306.08686](#)].
- [49] **ATLAS** Collaboration, G. Aad et al., *Search for long-lived, massive particles in events with displaced vertices and multiple jets in pp collisions at $\sqrt{s} = 13$ TeV with the ATLAS detector*, *JHEP* **2306** (2023) 200, [[arXiv:2301.13866](#)].
- [50] M. Bauer, M. Neubert, S. Renner, M. Schnubel, and A. Thamm, *Flavor probes of axion-like particles*, *JHEP* **09** (2022) 056, [[arXiv:2110.10698](#)].
- [51] **ATLAS** Collaboration, G. Aad et al., *Search for new phenomena in events with two opposite-charge leptons, jets and missing transverse momentum in pp collisions at $\sqrt{s} = 13$ TeV with the ATLAS detector*, *JHEP* **04** (2021) 165, [[arXiv:2102.01444](#)].
- [52] **CMS** Collaboration, V. Khachatryan et al., *Search for anomalous Wtb couplings and flavour-changing neutral currents in t-channel single top quark production in pp collisions at $\sqrt{s} = 7$ and 8 TeV*, *JHEP* **02** (2017) 028, [[arXiv:1610.03545](#)].
- [53] N. D. Christensen and C. Duhr, *FeynRules - Feynman rules made easy*, *Comput. Phys. Commun.* **180** (2009) 1614–1641, [[arXiv:0806.4194](#)].
- [54] A. Alloul, N. D. Christensen, C. Degrande, C. Duhr, and B. Fuks, *FeynRules 2.0 - A complete toolbox for tree-level phenomenology*, *Comput. Phys. Commun.* **185** (2014) 2250–2300, [[arXiv:1310.1921](#)].

- [55] C. Degrande, C. Duhr, B. Fuks, D. Grellscheid, O. Mattelaer, and T. Reiter, *UFO - The Universal FeynRules Output*, *Comput. Phys. Commun.* **183** (2012) 1201–1214, [[arXiv:1108.2040](#)].
- [56] **Particle Data Group** Collaboration, R. L. Workman et al., *Review of Particle Physics*, *PTEP* **2022** (2022) 083C01.
- [57] J. Alwall, M. Herquet, F. Maltoni, O. Mattelaer, and T. Stelzer, *MadGraph 5 : Going Beyond*, *JHEP* **06** (2011) 128, [[arXiv:1106.0522](#)].
- [58] J. Alwall, R. Frederix, S. Frixione, V. Hirschi, F. Maltoni, O. Mattelaer, H. S. Shao, T. Stelzer, P. Torrielli, and M. Zaro, *The automated computation of tree-level and next-to-leading order differential cross sections, and their matching to parton shower simulations*, *JHEP* **07** (2014) 079, [[arXiv:1405.0301](#)].
- [59] J. Alwall et al., *A Standard format for Les Houches event files*, *Comput. Phys. Commun.* **176** (2007) 300–304, [[hep-ph/0609017](#)].
- [60] T. Sjöstrand, S. Ask, J. R. Christiansen, R. Corke, N. Desai, P. Ilten, S. Mrenna, S. Prestel, C. O. Rasmussen, and P. Z. Skands, *An introduction to PYTHIA 8.2*, *Comput. Phys. Commun.* **191** (2015) 159–177, [[arXiv:1410.3012](#)].
- [61] M. Czakon and A. Mitov, *Top++: A Program for the Calculation of the Top-Pair Cross-Section at Hadron Colliders*, *Comput. Phys. Commun.* **185** (2014) 2930, [[arXiv:1112.5675](#)].
- [62] L. Lonnblad, *Correcting the color dipole cascade model with fixed order matrix elements*, *JHEP* **05** (2002) 046, [[hep-ph/0112284](#)].
- [63] R. D. Ball et al., *Parton distributions with LHC data*, *Nucl. Phys. B* **867** (2013) 244–289, [[arXiv:1207.1303](#)].
- [64] *ATLAS Pythia 8 tunes to 7 TeV data*, tech. rep., CERN, Geneva, 2014. All figures including auxiliary figures are available at <https://atlas.web.cern.ch/Atlas/GROUPS/PHYSICS/PUBNOTES/ATL-PHYS-PUB-2014-021>.
- [65] B. C. Allanach, M. Badziak, G. Cottin, N. Desai, C. Hugonie, and R. Ziegler, *Prompt Signals and Displaced Vertices in Sparticle Searches for Next-to-Minimal Gauge Mediated Supersymmetric Models*, *Eur. Phys. J. C* **76** (2016), no. 9 482, [[arXiv:1606.03099](#)].
- [66] M. Cacciari, G. P. Salam, and G. Soyez, *FastJet User Manual*, *Eur. Phys. J. C* **72** (2012) 1896, [[arXiv:1111.6097](#)].
- [67] G. Cottin, N. Desai, S. Kraml, and A. Lessa, “LLP Recasting Repository. <https://github.com/llprecasting/recastingCodes/>, 2019.”.